Technical

Use of advanced microscopy to elucidate structure, mechanism of crosslinking rubber

By Gina Butuc, Kees van Leerdam, Brenda Rossenaar
Nouryon Polymer Specialties

Auke Talma and Anke Blume
University of Twente

Material selection is governed by the properties the material must exhibit. The requirements for these macroscale properties can be very diverse and are sometimes conflicting. Examples of such properties are mechanical strength, visual appearance, electric conductivity, adhesion, wear, release profile, permeability and activity.

TECHNICAL NOTEBOOK
Edited by John Dick

The properties of a material are largely determined by the chemicals involved and the processing steps they have undergone. Rubber compounds consist of a balanced set of ingredients, including a polymeric phase and many additives like stabilizers, fillers, colorants, flame retardants and lubricants, as well as curatives. During processing, dispersing of various rubber components takes place, in which the original ingredients may react, degrade, migrate, change in crystallinity or are removed from the formulation due to dissolution or vaporization. Additional reactions take place during the curing process. Some of these effects may take place at scales beyond the visual level, which translates to the micrometer or nanometer scale.

In the development of materials with improved properties, analytical information on the test substance is very helpful for a focused approach. Knowledge on what has been made, or released, stimulates the thinking on steps to improve a product. Also, for failure analysis, quality control and in the regulatory field, analytical information is of value.

The number of analytical techniques applicable to rubbers and polymers is very broad. Often a combination of techniques is required to elucidate what is aimed for. Spectroscopic (e.g. IR, NMR, mass spectroscopy), chromatographic (gas or liquid based) and thermal analysis (e.g. DSC, TMA) techniques find many uses in rubber and polymer characterization.[1,2]

Microscopic techniques are employed to a lesser degree. Microscopy is most often used to determine the distribution of phases in polymers and rubber compounds, like the mixing of two or more polymers or the distribution of fillers like carbon black or silica. Often distributions are generated in a 2-dimensional plane. In recent years 3D-imaging of materials at several levels of detail has shown enormous progress.[3-5] Multi-technique imaging on a single position (correlative or hyphenated imaging) also adds new dimensions in the understanding of a material.[6]

Even less often microscopy has been used in rubber and polymer analysis to study mechanistic processes.

Depending on the definition, microscopy covers a broad field of imaging techniques, providing information on the structure and morphology of materials and on the local nature of the chemicals and their reactivity. Optical and electron microscopy (combined with EDX) are the most common microscopy techniques. The imaging modes of more spectroscopic techniques like IR, Raman, XPS and ToF-SIMS can also be considered part of the microscopy field, as well as techniques using other probes (AFM, X-ray, etc.).

This paper highlights some recent instrumental and material developments in the area of rubber compounds and polymers making use of these microscopic techniques.

Experimental and instrumental aspects

To study the distribution of the phases in a polymer blend, cross-sections are investigated, or thin slices, rather than topview inspection of sheets to avoid surface artifacts due to phase separation. Depending on the state of the blend, sectioning is done either at room temperature or under cryogenic conditions using an ultramicrotome (Leica UC7). Care has been taken to ensure that after sectioning no additional surface migration is taking place as a result of the presence of low molecular weight components. Surface migration, or emission of volatiles, is at higher risk when a sectioned polymer is investigated in vacuum (e.g. SEM). Also the interaction with an analyzing beam (light, electrons) might disturb the information on the blend, in particular when crosslinking is not yet complete.

SEM analysis was done with a Zeiss CrossBeam 540, equipped with an Oxford Instruments X-Max^N 150 silicon drift detector (SDD) for EDX (using Aztec software). ATLAS 5, a correlative workflow software, was used for large area imaging and slice-and-view experiments for tomography.

Scanning transmission electron microscopy (STEM) was done with a ThermoFisher Scientific Talos F200X G2, operated at 200 keV. The microscope is equipped with a Ceta camera for TEM imaging and a bright field and high-angle angular dark field detector for STEM imaging. Compositional analysis and mapping were performed by four in-column SDD Super-X detectors. Data acquisition and analysis was done with the Thermo Scientific Velox software.

The instrument used for imaging Raman was an AFM-Raman confocal spectrometer by WITec, model Alpha300RA+. The AFM features a digital pulse force mode (DPFM), a lateral resolution of < 10 nm, Z-resolution: < 1 nm and image size of 0.2-90 µm. The Raman spectrometer is used in conjunction with the AFM, which allows chemical composition identification. The operating wavelength ranges from 532 and 785 nm excitation, a surface mapping of rough samples by white light interference displacement sensor for proper focusing of laser beam with a lateral resolution of 1 µm.

Case study 1: Phase distribution and crosslinking in a rubber blend

In a search for polymeric materials with improved properties recently, the combination of ethylene propylene diene terpolymer (EPDM) rubber and a new polysulfide have been explored. EPDM is known for its good mechanical properties and good heat and ozone resistance. Polysulfides are known to have a high resistance against swelling in hydrocarbon oils and solvents. As a polysulfide a new material, a cyclic tetrasulfide (CTS) with relatively low molecular weight, is explored (**Fig. 1**). The resulting

Executive summary

Understanding the microstructure of materials such as rubber and thermoplastics can help design materials' macrostructure properties. Microscopy can provide useful information in designing soft materials such as rubber compounds, starting with understanding the reinforcing filler's dispersion in the elastomer matrix. Advanced microscopy instrumentation can go far beyond this dispersion characterization. Scanning and transmission electron microscopy (SEM and (S)TEM) coupled with energy-dispersive X-ray spectroscopy (EDX) are useful instrumentation used in phase characterization of soft materials.

Complementary insights on the presence of phases and the sulfur crosslinking process can be provided by imaging Raman spectroscopy. Case studies of rubber and polymer blends showcase the experimental challenges for the microscopist and demonstrate that the usage of microscopy goes one step beyond and provides crucial mechanistic, structure and performance-related information.

The main focus of this paper is to showcase various microscopy techniques used in elucidating the mechanism of ZnO and stearic acid of sulfur crosslinking and the polymeric phase morphology of a rubber blend.
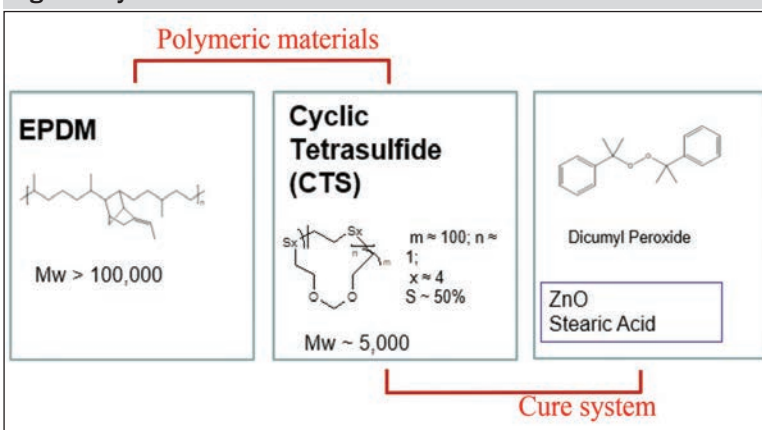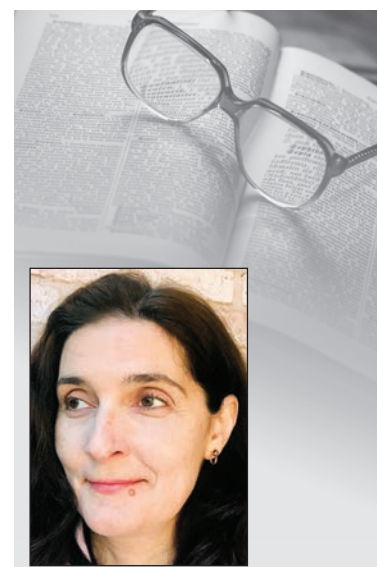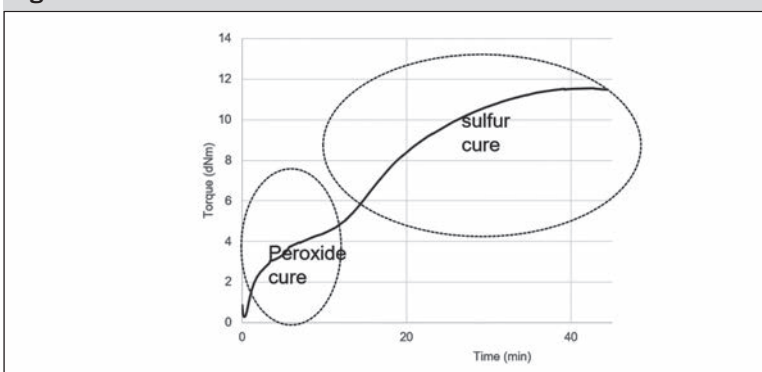
Butuc

The authors

Gina Butuc is a technical development manager at Nouryon Polymer Specialties. She has more than 25 years of experience in the polymer field, either polymer synthesis or application development and polymer testing, ranging from bench chemist to business management.

She is the inventor or co-inventor of seven U.S. and international patents and the author of eight technical articles and two book chapters.

Butuc holds a doctorate in elastomer technology engineering from the University of Twente in the Netherlands. She also earned a master's in organic chemistry and a bachelor's in physical chemistry, both from the University of Bucharest in Romania.

Kees van Leerdam is an analytical scientist, specializing in the expertise area of microscopy and surface analysis. He has worked in different science-related roles in the chemical industry (initially AkzoNobel, now Nouryon) for more than 30 years, serving many different markets, such as catalysis, fibers, pharmacy, mining, paper, coatings and polymers. In parallel, van Leerdam is currently coordinating analytical studies for REACH regulation in the European Union.

He holds a doctorate in applied physics on surface analysis from the Eindhoven University of Technology (NL), and a master's in chemistry on catalysis from Utrecht University (NL).

Fig. 1: Polymers and additives used to make EPDM-CTS blends.

Fig. 2: EPDM-CTS rheometer data.

Fig. 3: Imaging of EPDM-CTS blends by several microscopic techniques a) optical b) SEM c) SEM-EDX and d) Raman (hyphenated with SEM).
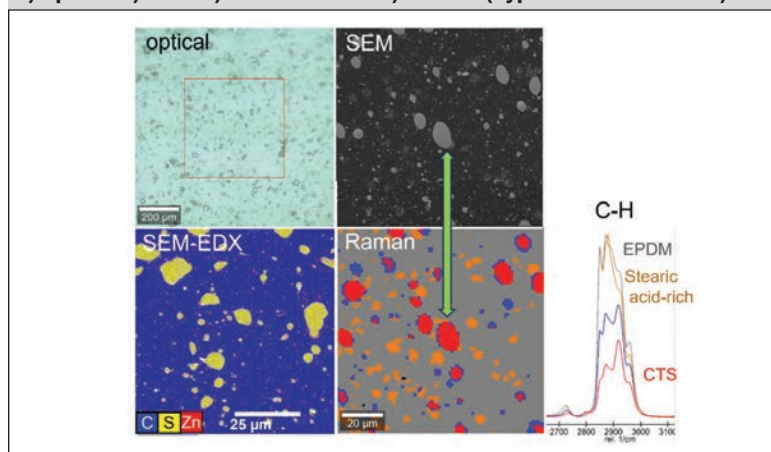
Technical

EPDM-CTS blend is targeted to have improved mechanical properties and resistance against swelling in hydrocarbon oil and solvents, as compared to rubber compound made of EPDM alone.

A possible advantage of using CTS is that it might exhibit a double function in the polymerization process. Firstly, CTS chain extension may occur after ring opening, resulting in a polysulfide polymer. As a second effect, the in-situ generation of S-species during curing may contribute to additional crosslinking of EPDM as compared to organic peroxides alone (dual cure).

Sulfur vulcanization of EPDM elastomers is usually performed in the presence of activators (ZnO and stearic acid) and accelerators (eg MBT, TMTD, ZDMC). In this study the formulation was stripped to a bare minimum to avoid potential interferences with additives other than the polymeric materials and the cure system. The effects of mixing conditions, curing times and curing temperatures on the rubbers have been investigated.[7]

Cyclic tetrasulfide (CTS) is produced by Nouryon Functional Chemicals and commercialized under the tradename of Thioplast CPS200. It is a low molecular weight oligomer, Mw ~5,000 and has a high sulfur content—50 percent.[8]

EPDM is produced by Arlanx-eo and commercialized under the trade name of Keltan 2450. This elastomer has a low Mooney viscosity ML (1+4) @ 125ºC of 28 and a relatively high ethylene content of 48 percent, while the ethylene norbornene content is 4.1 percent. Crosslinking agents are as follows:

• Dicumyl peroxide (40 wt. percent) on clay produced by Nouryon and commercialized under the trade name of Perkadox BC-40K-pd, in powder form;

• ZnO technical grade by Spectrum Chemicals; and

• Stearic acid technical grade by Spectrum Chemicals.

Compound mixing was performed in a C.W. Brabender internal mixer with a capacity of 0.3 liters and intermesh rotors, at 40-60 rpm and 70 percent fill factor. The resulting compound was flattened into a sheet using a 6-inch x 13-inch two-roll mill by Reliable Rubber & Plastic Machinery Co. The nip gap was 20mm, and the shear between the front roll and the rear roll was set at 1:1.75 range.

Alpha Technology moving die rheometer (MDR) 2000 was used for assessing crosslink density of rubber compounds; the rheometer data was recorded at 175ºC.

In these new types of blends several structure-related parameters are considered of interest for their performance. Early information on the overall crosslinking of EPDM and CTS rubber blend came from the rheometer collected data, which indicated a two-step cure, per **Fig. 2**. This indicates a rapid initial onset that is characteristic for organic peroxide cure followed by a slower slope increased in torque, which is characteristic for sulfur cure.

Additional information on polymeric phase distribution and cure information can be assessed by NMR, Raman and mass spectrometry.[9] In this section, the hyphenated use of microscopic techniques to determine the distribution of the phases in the polymers is discussed, as well as
See **Microscopy**, *page 20*
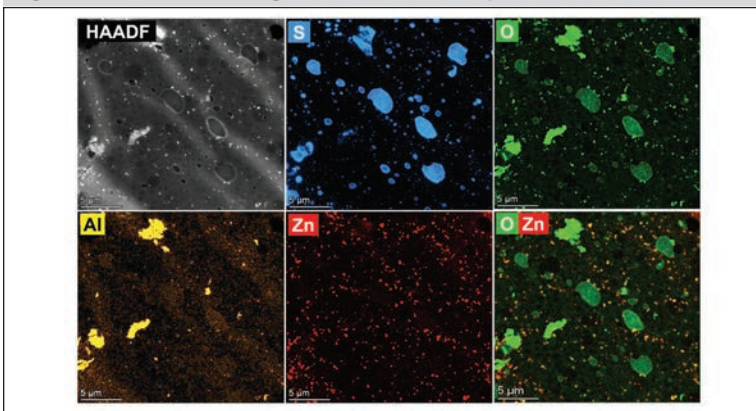
Fig. 5: STEM-HAADF images and elemental maps of ZnO in uncured EPDM-CTS blends and after curing.

Fig. 4: STEM-HAADF image and elemental maps of EPDM-CTS blend.
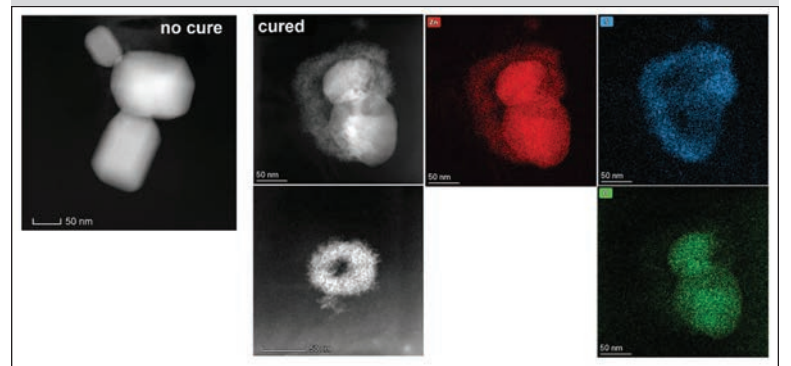
Fig. 6: STEM-HAADF image of the interface EPDM-CTS (pink arrow: ZnS, yellow arrow: Zn-stearate).

Microscopy

Continued from page 19

the efforts to obtain mechanistic information on the role of the activators ZnO and stearic acid.

The phase distributions in EPDM-CTS blends with different degrees and conditions of curing were imaged by optical microscopy, SEM (+EDX), and imaging Raman.[7] These techniques demonstrate that for EPDM-CTS sheets consisting of 75 phr EPDM, the EPDM phase is the continuous phase, in which CTS is dispersed as spherical domains with dimensions in the micrometer scale (**Fig. 3**). In optical and scanning electron microscopy the contrast difference between these polymers is sufficient to differentiate easily between them on a general level, due to the differences in their average chemical composition. Spatially resolved chemical analyses by SEM-EDX (identifying elements) and imaging Raman (identifying bonds) confirm the presence of an S-species in these domains. Since Raman spectrometry is sensitive for the type of sulfur containing species, this is a valuable method for determining chemical modifications of CTS.

When the same area is probed with SEM and imaging Raman (hyphenation) for an EPMD-CTS blend, the images appear to differ in several aspects. Some polysulfide domains are clearly visible in SEM, while not identified in Raman and vice versa. This is attributed to the differences in probing depth, which is deeper for Raman (microscale versus nanometer scale).

Imaging Raman, as processed by cluster analysis, shows domains which are enriched in stearic acid as compared to the average EPDM chemical composition (C-Hx at ~2,900 cm⁻¹), which are not detected by SEM-EDX, although—once identified by Raman—it can be visually seen in SEM as slightly brighter areas than EPDM. In the case of SEM-EDX this signal is lost in the overall C matrix signal from EPDM. Apparently, in the current case of short curing, local enrichments of stearic acid are present in the blend.

Another difference between the SEM-EDX data and imaging Raman is that Raman classifies an additional phase at the interface between the CTS island and the EPDM matrix, which is intermediate in chemical composition between CTS and EPDM. However, this is not observed in SEM-EDX. This raises the question whether the interfacial layer is real or is an artifact related to the relatively limited spatial resolution of imaging Raman. One more difference is that imaging Raman identifies small spots of a sulfide, which can originate from either a C-S or a Zn-S bond. SEM-EDX on its hand does show a distribution of very small Zn species which is not fully in line with the sulfide as identified by Raman. The situation is even more complicated by the fact that in Raman, overlap occurs between ZnO and S-S region around 437 cm⁻¹. [10,11]

As these features are too small to be analyzed in much more detail by either SEM-EDX or imaging Raman, STEM-EDX was applied. The lateral and depth resolution of STEM-EDX is much better due to the smaller beam size and use of thin slices of the rubber rather than taking cross-sectioned material. An additional advantage is also that the local chemical composition of the EPDM matrix can be determined much more accurately, which might reveal whether in addition to CTS phase separation, S-crosslinking of EPDM also is taking place.

Fig. 4 shows a STEM-HAADF image and corresponding elemental maps of an uncured EPDM-CTS blend at a five times higher magnification than the SEM and Raman images. At this magnification the lateral resolution is usually determined by the pixel size rather than the beam size or the thickness of the sample. The CTS domains are represented by the S and O enrichments, as expected from the chemical composition of CTS. Zn appears clearly present as small, oxidic particles, rather well distributed in the continuous EPDM phase, rather than being located in the CTS domains or at the interface between EPDM and CTS.

At higher magnifications the shape and chemical composition of individual ZnO particles in the EPDM matrix has been determined. In uncured blends the ZnO particles show well-defined, crystalline particles with sizes in the 50-200 nm range (**Fig. 5**). These particles have the typical characteristic of ZnO. Their chemical composition, as determined by STEM-EDX, shows an atomic Zn:O ratio of 1 and also the crystal structure is in line with the wurtzite hexagonal prism structure of ZnO, as derived from the lattice spacings (a.o. 0.25 nm for the 001 plane).

After curing, the morphology and chemical composition of these ZnO crystallites has clearly changed (**Fig. 5**). Frequently, a shell consisting of small nanoparticles (~3 nm in size) has grown around a ZnO core. These nanoparticles appear to be ZnS (EDX). The shell thickness is tens of nanometers. Furthermore, there seems to be some spacing present between the ZnO core and the ZnS shell. In other cases, the ZnO core has disappeared completely, leaving an empty space within the ZnS shell.

These results clearly indicate that some S-species originating from CTS is able to migrate into the EPDM matrix and react with Zn. The fact that the ZnS shell does not seem to grow directly on the surface of ZnO is an indication that Zn first dissolves, and maybe participates in other reactions, before it forms ZnS.

Normal TEM and STEM images of a thin slice are projections of the cumulative mass within the slice, which typically has a thickness between 20-100 nm. Depending on the orientation of the feature of interest, this may obscure finer details within the projected volume. In the present case, the images are not fully conclusive whether there is an open space between the ZnO core and the ZnS shell in all directions. This may be overcome by (S)TEM tomography, in which the slice is imaged under many angles in a tilt series, allowing for a three-dimensional reconstruction of the object of interest (back-projection). The reconstructed object can then be evaluated in any direction and with any thickness. This kind of analyses has been started.

In cured EPDM-CTS blends the interface between the CTS domains and the EPDM phase contains many clusters with small ZnS particles (**Fig. 6**). As for uncured blends, hardly any Zn enrichment is observed at the CTS-EPDM interface. This is an indication that during curing Zn can migrate along larger distances in the EPDM matrix than was observed for the distance between the ZnO core and its surrounding shell. It can be hypothesized that the local level of mobile S-species has an impact on the degree of conversion of ZnO or mobile Zn. This may imply that conversion levels may be higher around the CTS domains. This might have an impact on the degree of crosslinking. If so, the dispersion of the CTS domains may affect the properties of the film.

In the cured blends, S is also identified within the EPDM polymer, at a level below 1 percent, which is clearly higher than for the uncured system. This S signal is much less sensitive to electron beam irradiation than it is observed for the CTS domains. This is an indication that S has reacted with EPDM, possibly to form crosslinks.

As already demonstrated by SEM and imaging Raman, local enrichments related to stearic acid are present in the EPDM phase of cured CTS-EPDM blends. These enrichments are easily overlooked in (S)TEM due to their low contrast as compared to ZnO and ZnS. **Fig. 7** shows a STEM-HAADF image of an area with mainly EPDM in uncured EPDM-CTS at elevated brightness level. The image shows that around many ZnO particles an additional, platelike phase is present, which shows a bit more contrast than the low-contrast EPDM phase. According to EDX, these platelets contain a low, but detectable level of Zn (**Fig. 7**), suggesting that these platelets are Zn-stearate. This also explains why this phase has more contrast than EPDM itself. These platelets closely resemble featherlike zinc stearate platelets as identified in paint applications.[12]

Dark spherical holes (blue arrows) in the image are due to holes in the thin carbon substrate film. These results indicate that Zn stearate appears to be formed in the compound already during mixing time, and also during curing. Mechanistically, this would translate in either dissolution of Zn ions from ZnO followed by migration and reaction with stearic acid or direct abstraction of Zn

Fig. 7: STEM-HAADF image and Zn map of uncured EPDM-CTS, demonstrating the presence of Zn-stearate (yellow arrow) around ZnO (red arrow). Blue arrows indicate holes in the carbon support.
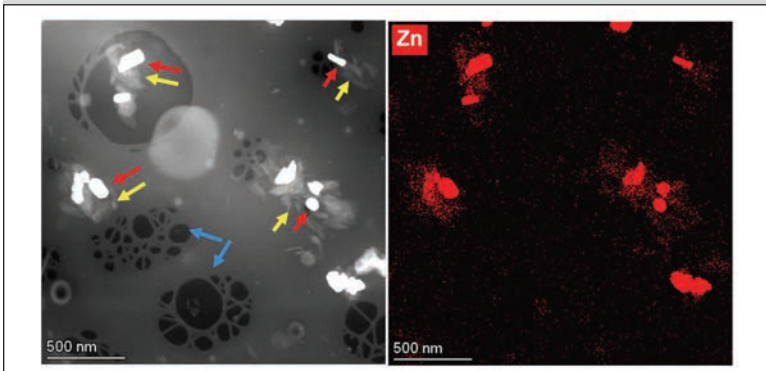

Fig. 8: TEM images of different conductive agents showing the different morphologies.

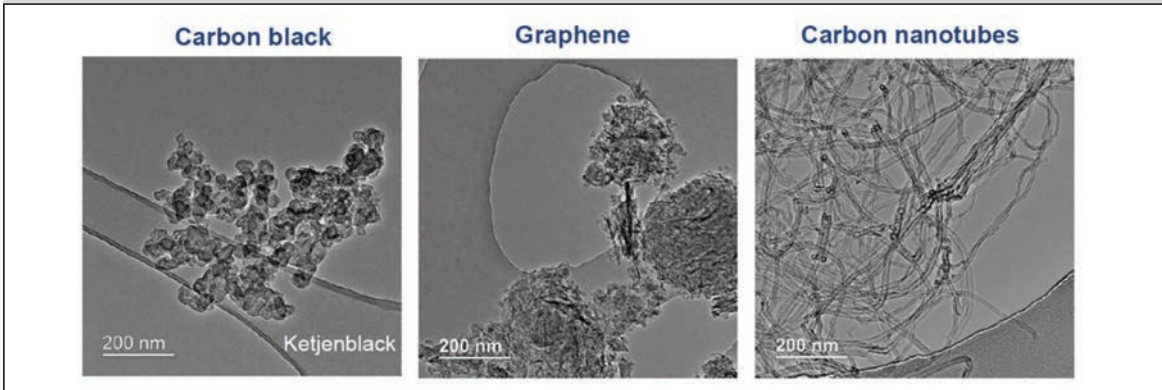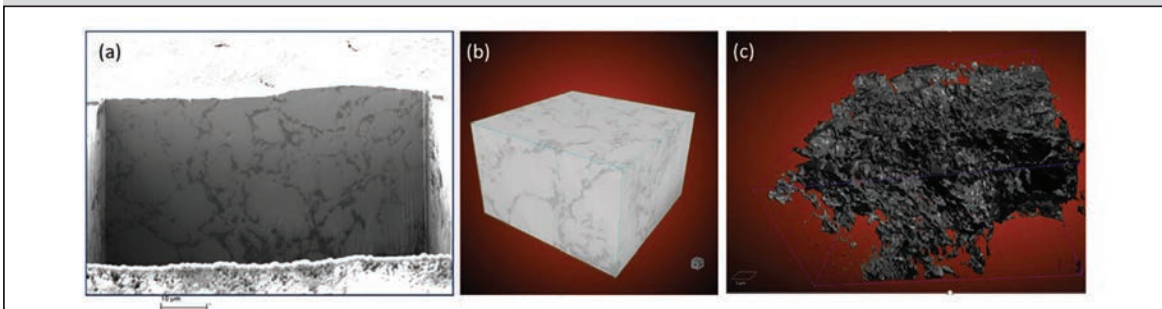Carbon black | Graphene | Carbon nanotubes

Fig. 9: SEM images of Ketjen black distribution in halogenated polymer. (a) SEM image of freshly prepared FIB cross section; (b) 3D reconstruction of series of 2D images, where the darker part represents the CB; (c) snapshot of a movie of segmented data cube (CB only).

Scheme 1: Proposed mechanism for ZnO-based CTS ring opening and reaction with EPDM.[13].
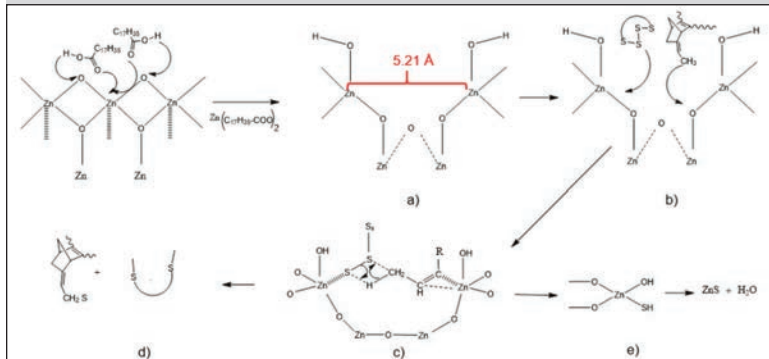
Scheme 2: Schematic representation of slice and view set up (a) top view (b) side view.
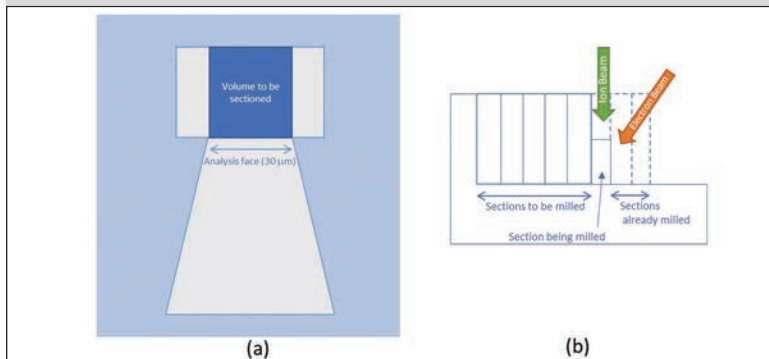
Technical

from ZnO by stearic acid. Moreover, the compatibility of Zn stearate with EPDM appears to be such that under these conditions phase separation is taking place.

These analyses provided insightful information related to the ZnO influence on sulfur crosslinking. The proposed mechanism is shown in **Scheme 1**.[13] In the first step, one $Zn2+$ is abstracted by stearic acid from the ZnO crystal structure in the form of Zn stearate. This leaves behind an active site or "template" on the ZnO crystal. The tetrasulfidic group of the CTS and the allylic group from the EPDM are fitted in the "template" area, as indicated in step b).

A complex interaction between adjacent Zn ions, the tetrasulfidic group and the allylic group is formed, as indicated in the step c). From this intermediate, the reaction progresses into two steps: d) CTS ring opening of the tetrasulfidic group and attaching to the allylic group of EPDM and one S atoms transferred to the Zn, and e) the remaining mostly inorganic portion of the complex formed in this step splits into ZnS and H_2O.

Case study 2: Carbon black distribution in a polymer

Carbon black is an additive present in a variety of polymers, resins and rubbers. It can act as a pigment, UV stabilizer, reinforcing filler, antistatic agent and electroconductive additive. Important parameters for the performance of carbon blacks are its structure (morphological and electronical), size, the degree of aggregation and the degree of purity, including the ability to be surface-modified to increase compatibility.

To achieve conductivity in polymers which are isolating by themselves, conductive pathways need to be established. **Fig. 8** compares the morphology of different types of materials in use as conductive additive. The conductive carbon black grade shown (Ketjenblack-brand from Nouryon) has a three-dimensional aggregate structure, graphene plates have a two-dimensional structure, while carbon nanotubes are mainly unidirectional shaped. The establishment of conductive pathways requires material-dependent dispersion and processing methods. Typical carbon black concentrations required for conductivity in many composites amount 3-15 wt. percent, the loading at which a composite becomes conductive, being called the percolation threshold.

TEM and AFM are the commonly used techniques to visualize the carbon black pathways in polymers[14], although also SEM, SAXS, SANS, near-field optical microscopy and Raman imaging have been applied.[15] However, due to limitations in the analysis techniques the number of published applications in rubbers is limited. Both TEM and AFM require advanced sample preparation (ultramicrotomy), often under cryogenic conditions, to obtain cross-sectioned material. Furthermore, the information in AFM is limited to the surface of the sectioned polymer. TEM, on its hand, has a limited field of view and projects the thickness of

a thin slice, which typically ranges between 20-150 nm. Both techniques thus basically deliver two-dimensional information. SEM is less often applied to study carbon black in rubbers as the contrast difference between those phases is very low, if so, determined by the fact that both materials mainly consist of carbon.

In this study SEM is used to visualize the carbon black distribution in a halogen-containing polymer. The presence of the halogen (increasing the average atomic number of the polymer) overcomes the contrast issue for this application.

The 2D SEM image (**Fig. 9a**) of a freshly created surface by using a focused ion beam (FIB) shows that the conductive carbon black in this polymer (the darker phase) is not randomly distributed, but forming a kind of network around domains of the polymer. However, based on this image alone it cannot be explained why the material is conductive; there seem to be gaps between the different carbon black (CB) strands.

In order to determine the three-dimensional distribution of the carbon black in the polymer. the combination of an FIB and a SEM can be used. The hyphenation of these ion and electron beams allows for repeated in-situ ion beam cutting of the mixture and subsequent SEM imaging. This serves as a basis for reconstruction of the distribution of the additive in the polymer.

Using this FIB-SEM slice-and-view technique (see **Scheme 2**) requires selection of the right settings for the purpose of the experiment.[16] This comprises a.o., the slice thickness controlled by

the FIB beam current in relation to the material properties and the probing depth as determined by the choice of detector. In the current case, best contrast vs. depth resolution was achieved by using the inLens Energy Selective Backscatter (ESB) detector of the SEM. Due to the presence of air voids between the individual carbon black particles, differences in milling rate are observed between areas below these voids and areas without these voids, which can lead to shadowing effects due to the created surface roughness (curtaining effect).

The effects of this curtaining on the SEM image are minimized by selecting the inLens ESB detector. Also, charging issues are circumvented by using this detector, while maximizing the resolution by only probing the outer few nm of the freshly prepared surface.

When individual 2D images collected via the slice-and-view FIB-SEM technique are combined to a 3D data cube (**Fig. 9b**) and the cube is segmented via image analysis into CB only (**Fig. 9c**), the three dimensional sponge-like interconnection of the individual CB agglomerates is obvious. Especially when the data cube is animated and rotated along the axis of the cube. This explains how the conductivity is achieved in this specific polymer. This knowledge can be used to predict the amount of CB necessary to achieve the percolation threshold.

Conclusions

Characterization of rubber compounds by imaging techniques is very helpful in relating macroscale properties to the dis-

tribution and reactivity of the chemicals present.

Information on the fate of the activators ZnO and stearic acid in EPDM-CTS mixtures led to a detailed proposal for the crosslinking mechanism. To visualize conductive pathways in insulators, the carbon black distribution was shown in three dimensions for a halogenated polymer.

Combining the use of imaging facilities with different specifications like resolution, depth information and type of species probed can lead to a detailed description of the rubber compound, including mechanistic information on the reactivity of components. Correlative microscopy and three-dimensional imaging further contribute to a more detailed understanding of the compound.
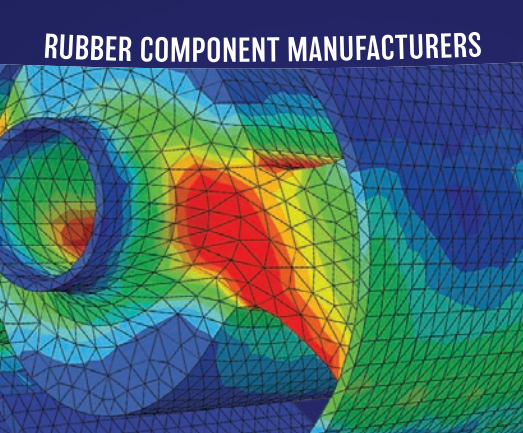
References

1. Forrest, M.J., 2018, Rubber Analysis: Characterisation, Failure Diagnosis and Reverse Engineering, Smithers Rapra, Shawbury, ISBN: 978-1-91108-840-0.
2. Loadman, M.J.R., 1998, Analysis of Rubber and Rubber-like Polymers, Springer, Dordrecht, ISBN: 978-94-010-5905-3.
3.. Vasarhelyi, L., Konya, Z., Kukovecz, A, Vajtai, R., 2020, Microcomputed tomography-based characterization of advanced materials: a review, Materials Today Advances, volume 8, 100084, https://doi.org/10.1016/j.mtadv.2020.100084.
4. Mobus, G. Inkson, B.J., 2007, Nanoscale tomography in materials science, Materials Today, volume 10(12), p. 18-25, https://doi.org/10.1016/S1369-7021(07)70304-3.
5. Hayashida, M., Malac, M., 2016, Practical electron tomography guide: Recent progress and future opportunities, Micron, volume 91, p. 49-74, https://doi.org/10.1016/j.micron.2016.09.010.
6. Burnett, T.L, McDonald, S.A., Gholinia, A., Geurts, R., Janus, M., Slater, T., Haigh, S.J., Ornek, C., Almuaili, F.M Engelberg, D.L., Thompson, G.E., and Withers, P.J., 2014, Correlative Tomography, Scientific reports, 4:4711, https://doi.org/10.1038/srep04711.
7. Butuc, S.G., 2021, PhD thesis, University of Twente, ISBN: 978-90-365-5315-5.
8. AkzoNobel Ethylene and Sulfur Derivatives, 2016, Product Data Sheet, Thioplast-brand CPS 200.
9. Butuc, G., Swart, J., Simons, M., Van Velde, J., Van Leerdam, K., Rossenaar, B., Talma, T., Blume, A., 2023, A fundamental study on Cyclic Tetrasulfide (CTS) as a sulfur donor and co-agent for rubber crosslinking, Rubber Chemistry and Technology, accepted paper.
10. Montenegro, D.N., Hortelano, V., Martınez, O., Martınez-Tomas, M.C., Sallet, V., Munoz-Sanjos, V., and Jimenez, J., 2013, Non-radiative recombination centers in catalyst-free ZnO nanorods grown by atmospheric-metal organic chemical vapor deposition, J. Phys. D: Appl. Phys. 46 235302, DOI 10.1088/0022-3727/46/23/235302.
11. McBrayer, J.D., Beechem, T.E., Perdue, B.R., Applett, C.A., Garzon, F.H., 2018, Polysulfide Speciation in the Bulk Electrolyte of a Lithium Sulfur Battery, J. Electrochem. Soc. 165 A876, DOI 10.1149/2.0441805jes.
12. Hermans, J.; Osmond, G.; van Loon, A.; Iedema, P.; Chapman, R.; Drennan, J.; Jack, K.; Rasch, R.; Morgan, G.; Zhang, Z.; Monteiro, M.; Keune, K., 2018, Electron Microscopy Imaging of Zinc Soaps Nucleation in Oil Paint, Microscopy and Microanalysis, 24(3), p. 318–322, https://doi.org/10.1017/S1431927618000387.
13. Butuc, S.G.; Van Leerdam, K.; Rossenaar, B.; Swart, J., Geurts, F., Bossinga-Geurts, B., Verwer, P., Talma, A., Blume, A., 2023, Elucidation of the role of ZnO in sulfur cure in novel EPDM-CTS blends, Polymer Testing, 117, 107843, https://doi.org/10.1016/j.polymertesting.2022.107843.
14. Conzatti, L., Costa, G., Falqui, L., and Turturro, A., 2009, Microscopic Imaging of Rubber Compounds, Rubber Technologist's Handbook, eds., White, J., De, S.K. and Naskar, K., Smithers Rapra, Volume 2, chapter 1, ISBN: 978-1-84735-099-2.
15. Moon, Y., Lee, H., Jung, J., Haewook, H., 2023, Direct visualization of carbon black aggregates in nitrile butadiene rubber by THz near-field microscope, Scientific Reports, 13:7846, https://doi.org/10.1038/s41598-023-34565-2.
16. Fager, C., Roding, M., Olsson, M., Loren, N., Von Corswant, C., Sarkka, A., and Olsson, E., 2020, Optimization of FIB–SEM Tomography and Reconstruction for Soft, Porous, and Poorly Conducting Materials, Microscopy & Microanalysis, Volume. 26 (4), p. 837-845, doi:10.1017/S1431927620001592.